From $J_{\text{eff}} = 1/2$ insulator to p-wave superconductor in single-crystal $Sr_2Ir_{1-x}Ru_xO_4$ ($0 \leqslant x \leqslant 1$)

S. J. Yuan,[1,*] S. Aswartham,[1] J. Terzic,[1] H. Zheng,[1] H. D. Zhao,[1] P. Schlottmann,[2] and G. Cao[1,†]

[1]*Center for Advanced Materials, Department of Physics and Astronomy, University of Kentucky, Lexington, Kentucky 40506, USA*

[2]*Physics Department, Florida State University, Tallahassee, Florida 32306, USA*

(Received 17 September 2015; revised manuscript received 3 November 2015; published 3 December 2015)

Sr_2IrO_4 is a magnetic insulator assisted by strong spin-orbit coupling (SOC) whereas Sr_2RuO_4 is a p-wave superconductor. The contrasting ground states have been shown to result from the critical role of the strong SOC in the iridate. Our investigation of structural, transport, and magnetic properties reveals that substituting $4d$ $Ru^{4+}(4d^4)$ ions for $5d$ $Ir^{4+}(5d^5)$ ions in Sr_2IrO_4 directly adds holes to the t_{2g} bands, reduces the SOC, and thus rebalances the competing energies in single-crystal $Sr_2Ir_{1-x}Ru_xO_4$. A profound effect of Ru doping driving a rich phase diagram is a structural phase transition from a distorted $I4_1/acd$ to a more ideal $I4/mmm$ tetragonal structure near $x = 0.50$ that accompanies a phase transition from an antiferromagnetic-insulating state to a paramagnetic-metal state. We also make a comparison with Rh-doped Sr_2IrO_4, highlighting important similarities and differences.

DOI: 10.1103/PhysRevB.92.245103 PACS number(s): 71.70.Ej, 75.30.Gw, 71.30.+h

I. INTRODUCTION

The $5d$-electron-based iridates have continuously attracted considerable interest as they display unusual properties primarily resulting from a delicate interplay between strong spin-orbit coupling (SOC) and other competing energies such as Coulomb interactions, noncubic crystalline electric fields, and Hund's rule coupling [1–3]. The $J_{\text{eff}} = 1/2$ insulating state is a manifestation of physics driven by such a new hierarchy of energies [1,2,4].

Among all the iridates studied, the single-layered Sr_2IrO_4 has been subjected to the most extensive investigations due to its $J_{\text{eff}} = 1/2$ insulating ground state, and similarities of its crystallographic, electronic, and magnetic structures to those of the undoped high-T_C cuprate La_2CuO_4. However, IrO_6 octahedra in Sr_2IrO_4 rotate about the c axis by about 12°; this distinct structural feature, which is absent in La_2CuO_4, critically affects the ground state of the iridate. Sr_2IrO_4 undergoes an antiferromagnetic (AFM) ordering at $T_N = 240$ K, and exhibits a canted magnetic structure that rigidly tracks the staggered rotation of the IrO_6 octahedra in Sr_2IrO_4 [5–8].

It is useful to first compare Sr_2IrO_4 with its isostructural $4d$-based counterparts Sr_2RhO_4 and Sr_2RuO_4. Their underlying structural and physical properties are listed in Table I for contrast and comparison. Both Sr_2IrO_4 and Sr_2RhO_4 crystallize in a reduced tetragonal structure with space group $I4_1/acd$ due to a rotation of the IrO_6 or RhO_6 octahedra about the c axis by ~12° or ~9.7°, respectively, resulting in an unit cell expanded by $\sqrt{2} \times \sqrt{2} \times \sqrt{2}$, as compared to the undistorted cell [9,10]. Despite the structural similarity, Sr_2RhO_4 is a paramagnetic (PM) correlated metal, sharply contrasting with the magnetic insulator Sr_2IrO_4 [5,6,9,11,12], owed chiefly to the weaker SOC (~0.15 eV), compared with the SOC (~0.4 eV) for Sr_2IrO_4, which renders a smaller splitting between the $J_{\text{eff}} = 1/2$ and $J_{\text{eff}} = 3/2$ bands [1,13]. On the other hand, Sr_2RuO_4 adopts an ideal tetragonal structure without the rotation of RuO_6 octahedra and supports a p-wave superconducting state [14]. Indeed, the impact of the SOC strongly depends on the detailed band structure near the Fermi surface E_F, the Coulomb interactions, and the lattice distortions [15–18], and this in part explains differences between the superconducting Sr_2RuO_4 and metallic Sr_2RhO_4 which is very close to the borderline of a metal-insulator transition.

In our previous work, we tuned the ground state by substituting Rh for Ir in Sr_2IrO_4, in an attempt to reduce the SOC [13]. This chemical substitution generates a rich phase diagram for $Sr_2Ir_{1-x}Rh_xO_4$($0 \leqslant x \leqslant 1$), where a robust metallic state is not fully established until x approaches 1 due in part to a variation of the valence state of Rh with x [13,19,20]. As a natural extension of this study, we have extended our investigation to Ru-doped Sr_2IrO_4 or $Sr_2Ir_{1-x}Ru_xO_4$. There have been several studies on structural, transport, and magnetic properties of $Sr_2Ir_{1-x}Ru_xO_4$ based on polycrystalline samples [21–24]. These studies certainly reveal valuable information about the system. However, given the nature of the layered crystal structure of $Sr_2Ir_{1-x}Ru_xO_4$, single-crystal samples are indispensable to fully and adequately address intrinsic properties of these materials.

In this paper, we report a thorough investigation of structural, transport, and magnetic properties of single-crystal $Sr_2Ir_{1-x}Ru_xO_4$ with $0 \leqslant x \leqslant 1$. Ru doping induces a structural phase transition from a distorted tetragonal structure with space group $I4_1/acd$ to a more ideal one with $I4/mmm$ near $x = 0.50$. It is this structural change that marks a concurrent phase transition from the AFM insulating state ($x < 0.50$) to a Ru-doping induced PM metallic state ($x > 0.50$). We also make a comparison between $Sr_2Ir_{1-x}Ru_xO_4$ and $Sr_2Ir_{1-x}Rh_xO_4$, highlighting important similarities and differences.

II. EXPERIMENT

The single crystals of $Sr_2Ir_{1-x}Ru_xO_4$ were grown from off-stoichiometric quantities of $SrCl_2$, $SrCO_3$, IrO_2, and RuO_2 using self-flux techniques. Similar technical details are described elsewhere [4,6,25,26]. The structures of the crystals were determined using a Nonius Kappa CCD x-ray diffractometer at 90 K. Structures were refined by full-matrix least squares

*Corresponding author: shujuan.yuan@uky.edu

†Corresponding author: cao@uky.edu

TABLE I. Comparison for Sr_2IrO_4, Sr_2RhO_4, and Sr_2RuO_4 [3].

Compound	Space group	SOC (eV)	Exemplary phenomena
Sr_2IrO_4	$I4_1/acd$	~0.40	Antiferromagnet / $J_{\text{eff}} = 1/2$ insulator
Sr_2RhO_4	$I4_1/acd$	~0.16	Paramagnet/metal
Sr_2RuO_4	$I4/mmm$	~0.15	Paramagnet / p-wave superconductor at low T

using the SHELX-97 programs [27]. All structures affected by absorption and extinction were corrected by comparison of symmetry-equivalent reflections using the program SADABS [27]. It needs to be emphasized that the single crystals are of high quality and there is no indication of any mixed phases in all the doped single crystals studied. The presence of any mixed phases or inhomogeneity in the single crystals would not allow any converging structural refinements. The standard deviations of all lattice parameters and interatomic distances are smaller than 0.1%. Chemical compositions of the single crystals were estimated using both single-crystal x-ray diffraction and energy-dispersive x-ray analysis (Hitachi/Oxford 3000). Magnetization and electrical resistivity were measured using either a Quantum Design MPMS-7 superconducting quantum interference device (SQUID) magnetometer and/or a physical property measurement system with 14-T field capability.

III. RESULTS AND DISCUSSION

The Ru ion tends to be tetravalent Ru^{4+} in perovskite ruthenates [3]. Substituting Ru^{4+} ($4d^4$) for Ir^{4+}($5d^5$) in Sr_2IrO_4 changes the crystal structure and adds holes to the t_{2g} bands. We first examine changes of the crystal structure in $Sr_2Ir_{1-x}Ru_xO_4$. Sr_2IrO_4 crystallizes in a distorted tetragonal structure with reduced space-group symmetry $I4_1/acd$ due to a rotation of the IrO_6 octahedra about the c axis by ~12° with the lattice parameters $a = b = 5.4773(8)$ Å and $c = 25.76(5)$ Å at $T = 90$ K. This rotation corresponds to a distorted in-plane Ir-O1-Ir bond angle θ (=156.474° at $T = 90$ K). In sharp contrast, Sr_2RuO_4 crystallizes in the ideal K_2NiF_4 structure with space group $I4/mmm$ featuring 180° Ru-O1-Ru bonds in the basal plane or no rotation of RuO_6 octahedra [10]. With increasing x, Ru doping initially weakens and eventually eliminates the structural distortions with a decrease in the lattice parameters on the a and c axes and the ratio of c/a, as shown in Fig. 1. More importantly, a structural transition from $I4_1/acd$ to $I4/mmm$ occurs near $x = 0.50$. The Ir/Ru-O1-Ir/Ru bond angle θ, reflecting the rotation of the octahedra about the c axis, increases with x and becomes 180° abruptly near $x = 0.50$, the structural transition [see Fig. 2(a)]. The in-plane bond length Ir/Ru-O1 shortens correspondingly with a sudden shortening at the structural transition as well; it then levels off with further increasing x, as shown in Fig. 2(b). On the other hand, the Ir/Ru-O2 bond length, which is more closely associated with the lattice parameter on the c axis, initially decreases with x, and then shows a sudden increase at $x = 0.50$ before decreasing again with further increase of x [see Fig. 2(c)]. For contrast and comparison, we also illustrate the lattice parameters of $Sr_2Ir_{1-x}Rh_xO_4$ [see Figs. 2(d)–2(f)]. Apparently, all the bond angles and bond lengths for Rh-doped samples show only slight changes with increasing x, sharply contrasting with those in the Ru-doped Sr_2IrO_4.

The electrical resistivity $\rho(T)$ of $Sr_2Ir_{1-x}Ru_xO_4$ for the a and c axes is drastically reduced by nearly five orders of magnitude at low temperatures as x is increased from $x = 0$ to 0.17, and a metallic state is induced at $x = 0.49$ [see Figs. 3(a) and 3(b)]. For $x \geqslant 0.49$, there is an upturn at low T in the a-axis resistivity $\rho_a(T)$. The temperature of the minimum is denoted with T^*, which decreases with x. A metal state is fully realized only at $x = 0.92$. This behavior is similar to that observed in $Sr_3(Ir_{1-x}Ru_x)_2O_7$; it is attributed to a robust Mott gap that blocks the charge transfer of doped holes [28]. As also presented by Glamazda *et al.* [29], the two Ir/Ru-O1-Ir/Ru bond angle modes with different Ir/RuO_6 octahedral rotations coexist and compete upon Ru doping, resulting in an electronic phase separation [29]. The c-axis resistivity ρ_c exhibits a different temperature dependence and larger magnitude, particularly for more heavily Ru-doped Sr_2IrO_4.

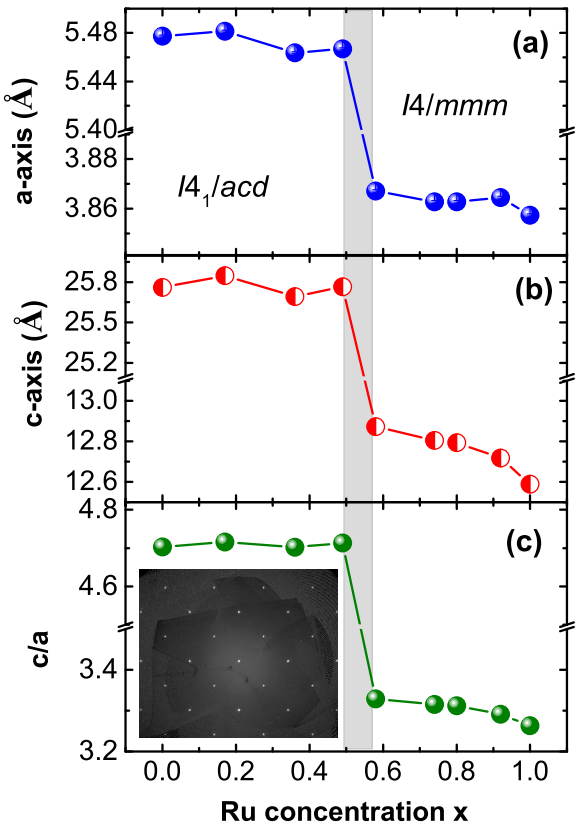

FIG. 1. (Color online) Ru concentration x dependence at $T = 90$ K of the lattice parameters of the a axis (a), the c axis (b), and the c/a ratio (c). Inset: Representative single-crystal Bragg diffraction peaks for the [001] direction; note the highly ordered crystal structure of $Sr_2Ir_{1-x}Ru_xO_4$. The shaded area indicates the region where the structural phase transition occurs.

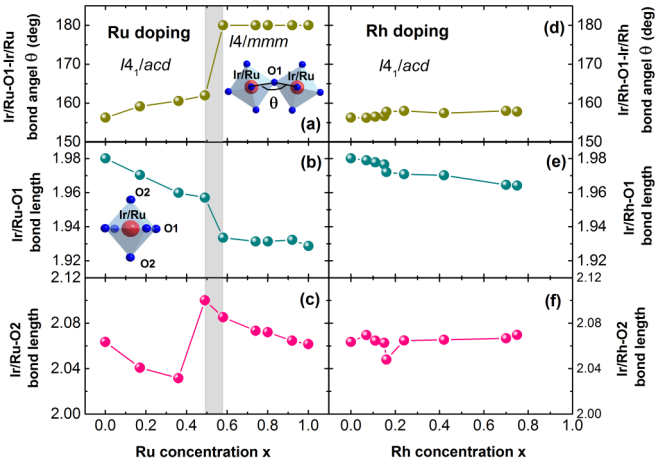

FIG. 2. (Color online) On the left panel, the Ru concentration x dependence at $T = 90$ K of (a) the Ir/Ru-O1-Ru/Ir bond angle θ, (b) the in-plane Ir/Ru-O1 bond length, and (c) the out-of-plane Ir/Ru-O2 bond length. The shaded area indicates the region where the structural phase transition occurs. For comparison, the right panel shows the Rh concentration x dependence of (d) the Ir/Rh-O1-Ir/Rh bond angle $fn\theta$, (e) the in-plane Ir/Rh-O1 bond length, and (f) the Ir/Rh-O2 bond length. The data for Rh doping are obtained from the crystals used in Ref. [13]. The insets show the definition of the bond angle Ir/Ru-O1-Ir/Ru, and the bond lengths Ir/Ru-O1 and Ir/Ru-O2.

The increased anisotropy in $\rho(T)$ suggests a two-dimensional nature of the electronic structure and is qualitatively consistent with the changes in the in-plane and out-of-plane Ir/Ru-O bond lengths [Figs. 2(b) and 2(c)]. It is remarkable that the resistivity exhibits no discernible effect due to disorder in $Sr_2Ir_{1-x}Ru_xO_4$. In contrast, for Rh substitution the system always remains in proximity to the insulting state. Each Ru atom adds one hole, which gives rise to a higher density of states near E_F; more

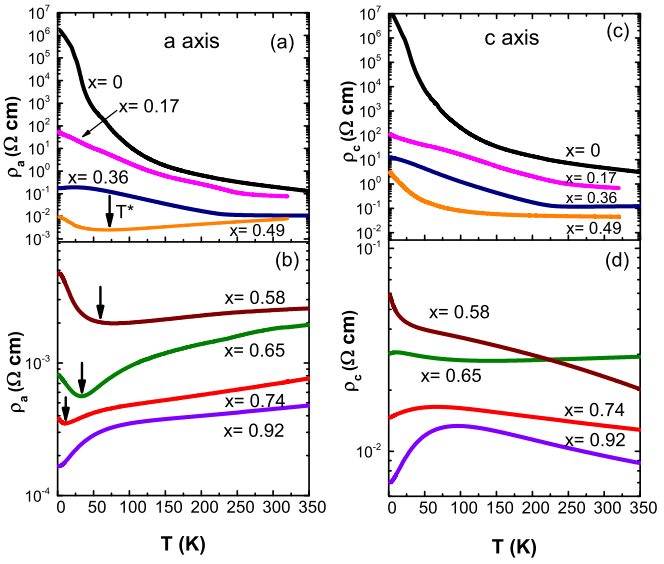

FIG. 3. (Color online) The temperature dependence of the resistivity $\rho(T)$ (a),(b) in the ab plane and (c),(d) along the c-axis for representative compositions $x = 0, 0.17, 0.36, 0.49, 0.58, 0.65, 0.74$, and 0.92. The arrows indicate the minimum of $\rho_a(T)$ defining T^*.

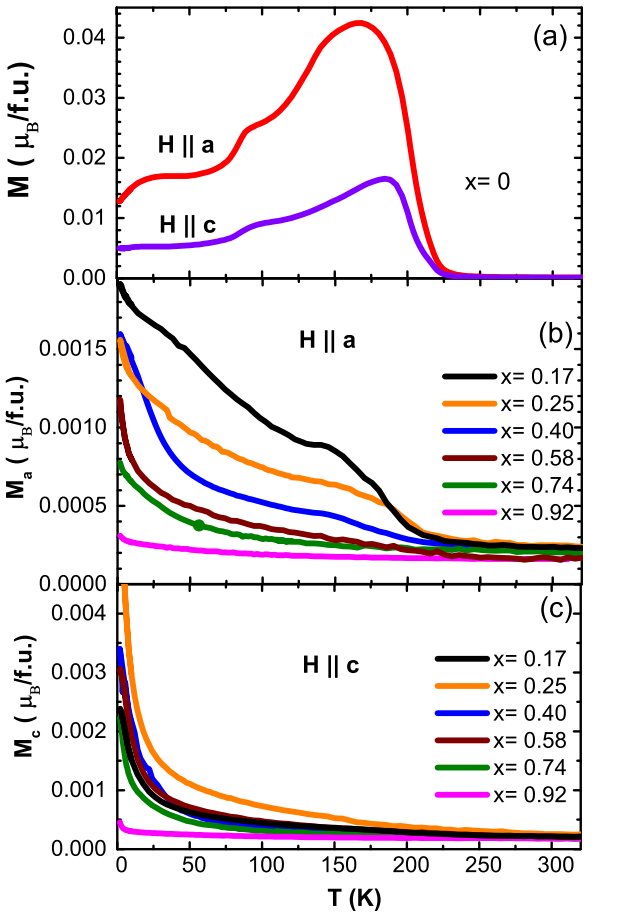

FIG. 4. (Color online) The temperature dependence at $\mu_0 H = 0.1$ T of the magnetization (a) M_a and M_c for $x = 0$, and (b) M_a and (c) M_c for the representative compositions $x = 0$, 0.17, 0.25, 0.40, 0.58, 0.74, and 0.92.

importantly, Ru doping drives a structural phase transition to an ideal tetragonal structure with no octahedral distortion, and thus enhances the electron hopping and supports a more robust metallic state in $Sr_2Ir_{1-x}Ru_xO_4$ when x approaches 1. Under these circumstances disorder in the alloy plays a less relevant role, in contrast to the situation in Rh-doped Sr_2IrO_4 in which Anderson localization dominates a wide range of Rh doping [13]. Nevertheless, the transport properties of Sr_2IrO_4 change more drastically with Ru doping, and this trend was observed and briefly discussed when compared to that of Rh-doped Sr_2IrO_4. The availability of additional single-crystal samples with more different Ru doping levels enables a more comprehensive study of $Sr_2Ir_{1-x}Ru_xO_4$, leading to a rich phase diagram (Fig. 7) discussed below.

The temperature-dependent magnetization $M(T)$ data for representative compositions of single crystals of $Sr_2Ir_{1-x}Ru_xO_4$ are presented in Fig. 4. There is a kink in $M(T)$ for $x = 0$ at 100 K that is attributed to a possible rearrangement of the magnetic order and is closely associated with the magnetoresistivity [30], the magnetoelectric effect [4], and unusual muon responses [31]. Ru doping suppresses the AFM transition T_N from 240 K at $x = 0$ to zero at $x = 0.49$. It needs to be pointed out that the AFM transition T_N for $0.40 < x < 0.49$ becomes less well defined; however, a close

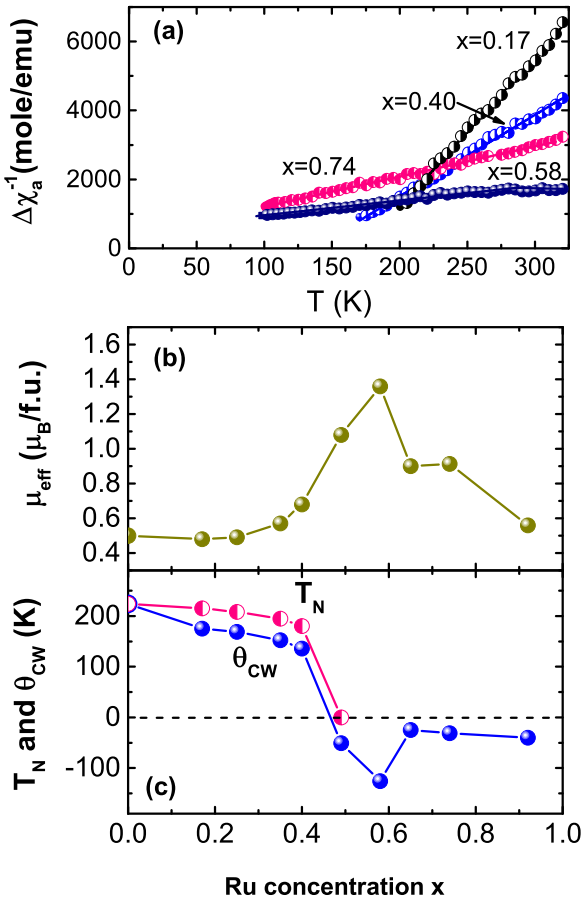

FIG. 5. (Color online) (a) The temperature dependence of magnetic susceptibility $\Delta\chi^{-1}$ for the representative compositions $x = 0.17$, 0.40, 0.58, and 0.74. The Ru concentration x dependence of (b) the magnetic effective moment μ_{eff}, and (c) T_N and θ_{CW}. Note the varying temperature intervals for the fit.

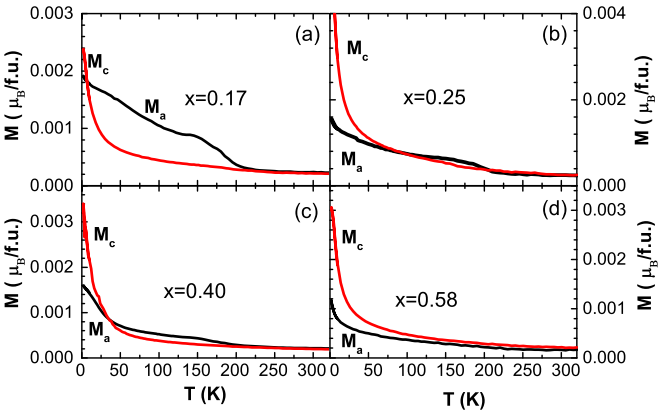

FIG. 6. (Color online) The temperature dependence at $\mu_0 H = 0.1$ T of the magnetization M_a and M_c for representative compositions (a) $x = 0.17$, (b) $x = 0.25$, (c) $x = 0.4$, and (d) $x = 0.58$. The magnetization was measured after field cooling at $\mu_0 H = 0.1$ T.

examination indicates that the T_N is not completely suppressed to zero until $x = 0.49$. Nevertheless, it is reasonably close to the classical (i.e., spin-only) two-dimensional site percolation threshold of $x = 0.41$ [32]. It is also noted that the AFM state vanishes at $x = 0.16$ in Rh-doped Sr_2IrO_4 or $Sr_2Ir_{1-x}Rh_xO_4$ [13]. The rapid suppression of the AFM state is attributed to a varying valence state of Ir and Rh ions and a change in the relative strength of SOC, tetragonal electric field effects, and Hund's rule coupling, which competes with the SOC and prevents the occurrence of the $J_{\text{eff}} = 1/2$ state [13,19].

We analyzed the magnetic data using the Curie-Weiss law $\chi = \chi_0 + C/(T - \theta_{\text{CW}})$ (where χ_0 is a temperature-independent constant, θ_{CW} the Curie-Weiss temperature, and C the Curie constant) and then used χ_0 to obtain $\Delta\chi = \chi - \chi_0 = C/(T - \theta_{\text{CW}})$ and $\Delta\chi^{-1}$ vs T, as shown in Fig. 5(a). Here, $C = (N_A/3k_B)\mu_{\text{eff}}^2$ with N_A being Avogadro's number and k_B the Boltzmann constant. The effective magnetic moment μ_{eff} per formula unit is then derived from C, as shown in Fig. 5(b). Note that the temperature range for the fit depends on x, but a high-temperature interval is used in every case. μ_{eff} remains essentially unchanged initially and then increases rapidly when $x > 0.49$, peaking at $x = 0.58$ before decreasing with further increasing x. The peak happens in the doping range where the structural phase transition takes place [see Figs. 2(a)–2(c)]. The Ru doping dependence of μ_{eff} is qualitatively consistent with the results in an earlier study on polycrystalline samples [21]. The Curie-Weiss temperature θ_{CW} tracks T_N for $0 \leqslant x \leqslant 0.49$, and then changes its sign from positive to negative as x increases further, as shown in Fig. 5(c). It is remarkable that the abrupt change in θ_{CW} also occurs in the range of the structural phase transition, echoing the sudden jump of μ_{eff}. θ_{CW} was obtained from a high-T fit and it is positive (ferromagnetic exchange) in the antiferromagnetic region, where $T_N > 0$. Note also that $\theta_{\text{CW}} = -126$ K for $x = 0.58$ where no long-range order exists. Since θ_{CW} measures the strength of the magnetic interaction, such a large absolute value of θ_{CW} in a system without magnetic ordering implies a strong magnetic frustration, which may primarily result from a competition between the AFM (Ir 5d electrons) and ferromagnetic (Ru 4d electrons) coupling.

Ru doping affects the magnetic anisotropy as well. The c-axis magnetization M_c becomes stronger than the a-axis magnetization M_a, especially at low temperatures, with increasing x (see Fig. 6 as well as Fig. 4). This behavior is absent in Rh-doped Sr_2IrO_4 but is observed in $Ca_2Ru_{1-x}Ir_xO_4$ due to the strong interaction between Ru 4d and Ir 5d electrons [33]. For $x = 0$, M_a is larger than M_c because the magnetic moment lies within the basal plane [7]. Upon Ru doping, M_c becomes larger than M_a at low temperatures initially and then throughout the entire temperature range measured for $x \geqslant 0.58$ (see Fig. 6). This change suggests a spin flop from the basal plane to the c axis due to Ru doping. Interestingly, Rh doping (up to $x = 0.12$) rearranges the in-plane magnetic configuration without any c-axis magnetic component [13].

The above evolution of the transport and magnetic properties closely follows the changes in the lattice properties. As illustrated in Figs. 2(a) and 2(b), Ru doping results in an increase in the Ir/Ru-O1-Ir/Ru bond angle and a decrease in the in-plane Ir/Ru-O1 bond length, which inevitably enhance the d-orbital overlap or electron hopping. These lattice changes along with added holes and reduced SOC explain the drastic decrease in the electrical resistivity (Fig. 3) and the vanishing AFM state.

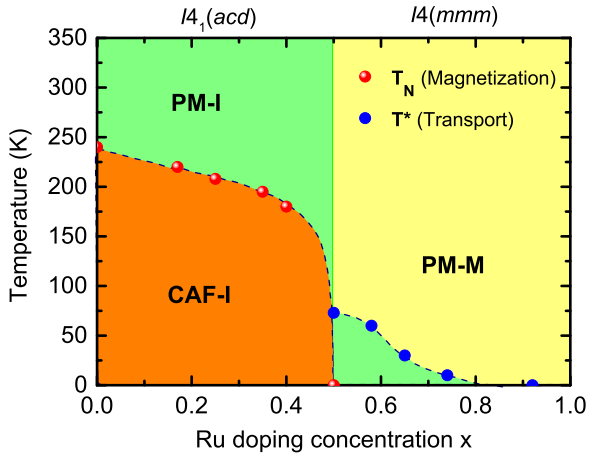

FIG. 7. (Color online) The phase diagram for $Sr_2Ir_{1-x}Ru_xO_4$ generated based on the data presented above. Note that CAF-I denotes the canted antiferromagnetic insulating phase, PM-I denotes the paramagnetic insulating phase, and PM-M indicates the paramagnetic metallic regime.

A phase diagram for $Sr_2Ir_{1-x}Ru_xO_4$ generated based on the data presented above summarizes the central findings of this study, as shown in Fig. 7. The most prominent feature of the phase diagram is the structural phase transition from a distorted $I4_1/acd$ to a more ideal $I4/mmm$ tetragonal structure near $x = 0.50$; this structural phase transition accompanies a magnetic transition from the canted-antiferromagnetic-insulating (CAF-I) to the paramagnetic-metal (PM-M) ground state. All results indicate that the $Ru^{4+}(4d^4)$ substituting for $Ir^{4+}(5d^5)$ adds holes into the t_{2g} bands and reduces SOC but it is the lattice degrees of freedom that primarily drive the rich phase diagram. Remarkably, this phase diagram contrasts with that of Rh-doped Sr_2IrO_4 (Fig. 5 in Ref. [13]) in which the AFM state vanishes more rapidly (at 16% Rh doping) but the insulating state is much more resilient to Rh doping, in part because of the rotation of RhO_6 octahedra in Sr_2RhO_4 that leads to a band folding and narrowing, giving rise to nearly degenerate states close to the Fermi level [17] and because of the varying valence state of both Rh and Ir that causes the Anderson localization [13,19,20].

ACKNOWLEDGMENTS

This work was supported by the National Science Foundation via Grant No. DMR-1265162 and by the Department of Energy (BES) through Grant No. DE-FG02-98ER45707 (P.S.).

[1] B. J. Kim, H. Jin, S. J. Moon, J. Y. Kim, B. G. Park, C. S. Leem, J. Yu, T. W. Noh, C. Kim, S. J. Oh, J. H. Park, V. Durairaj, G. Cao, and E. Rotenberg, Phys. Rev. Lett. **101**, 076402 (2008).
[2] B. J. Kim, H. Ohsumi, T. Komesu, S. Sakai, T. Morita, H. Takagi, and T. Arima, Science **323**, 1329 (2009).
[3] G. Cao and L. E. DeLong, in *Frontiers of 4d- and 5d-Transition Metal Oxides* (World Scientific, Singapore, 2013).
[4] M. Ge, T. F. Qi, O. B. Korneta, D. E. De Long, P. Schlottmann, W. P. Crummett, and G. Cao, Phys. Rev. B **84**, 100402 (2011).
[5] M. K. Crawford, M. A. Subramanian, R. L. Harlow, J. A. Fernandez-Baca, Z. R. Wang, and D. C. Johnston, Phys. Rev. B **49**, 9198 (1994).
[6] G. Cao, J. Bolivar, S. McCall, J. E. Crow, and R. P. Guertin, Phys. Rev. B **57**, R11039 (1998).
[7] F. Ye, S. Chi, B. C. Chakoumakos, J. A. Fernandez-Baca, T. Qi, and G. Cao, Phys. Rev. B **87**, 140406 (2013).
[8] S. Boseggia, R. Springell, H. C. Walker, H. M. Rønnow, C. Rüegg, H. Okabe, M. Isobe, R. S. Perry, S. P. Collins, and D. F. McMorrow, Phys. Rev. Lett. **110**, 117207 (2013).
[9] M. A. Subramanian, M. K. Crawford, R. L. Harlow, T. Ami, J. A. Fernandez-Baca, Z. R. Wang, and D. C. Johnston, Physica C: Superconductivity **235–240**, 743 (1994).
[10] Q. Huang, J. L. Soubeyroux, O. Chmaissem, I. N. Sora, A. Santoro, R. J. Cava, J. J. Krajewski, and W. F. Peck, Jr., J. Solid State Chem. **112**, 355 (1994).
[11] R. S. Perry, F. Baumberger, L. Balicas, N. Kikugawa, N. J. C. Ingle, A. Rost, J. F. Mercure, Y. Maeno, Z. X. Shen, and A. P. Mackenzie, New J. Phys. **8**, 175 (2006).
[12] S. J. Moon, M. W. Kim, K. W. Kim, Y. S. Lee, J. Y. Kim, J. H. Park, B. J. Kim, S. J. Oh, S. Nakatsuji, Y. Maeno, I. Nagai, S. I. Ikeda, G. Cao, and T. W. Noh, Phys. Rev. B **74**, 113104 (2006).
[13] T. F. Qi, O. B. Korneta, L. Li, K. Butrouna, V. S. Cao, X. Wan, P. Schlottmann, R. K. Kaul, and G. Cao, Phys. Rev. B **86**, 125105 (2012).
[14] Y. Maeno, H. Hashimoto, K. Yoshida, S. Nishizaki, T. Fujita, J. G. Bednorz, and F. Lichtenberg, Nature (London) **372**, 532 (1994).
[15] G. Jackeli and G. Khaliullin, Phys. Rev. Lett. **102**, 017205 (2009).
[16] C. Martins, M. Aichhorn, L. Vaugier, and S. Biermann, Phys. Rev. Lett. **107**, 266404 (2011).
[17] M. W. Haverkort, I. S. Elfimov, L. H. Tjeng, G. A. Sawatzky, and A. Damascelli, Phys. Rev. Lett. **101**, 026406 (2008).
[18] G.-Q. Liu, V. N. Antonov, O. Jepsen, and O. K. Andersen, Phys. Rev. Lett. **101**, 026408 (2008).
[19] J. P. Clancy, A. Lupascu, H. Gretarsson, Z. Islam, Y. F. Hu, D. Casa, C. S. Nelson, S. C. LaMarra, G. Cao, and Y.-J. Kim, Phys. Rev. B **89**, 054409 (2014).
[20] S. Chikara, D. Haskel, J.-H. Sim, H.-S. Kim, C.-C. Chen, G. Fabbris, L. S. I. Veiga, N. M. Souza-Neto, J. Terzic, K. Butrouna, G. Cao, M. J. Han, and M. van Veenendaal, Phys. Rev. B **92**, 081114 (2015).
[21] R. J. Cava, B. Batlogg, K. Kiyono, H. Takagi, J. J. Krajewski, W. F. Peck, L. W. Rupp, and C. H. Chen, Phys. Rev. B **49**, 11890 (1994).
[22] M. V. Rama Rao, V. G. Sathe, D. Sornadurai, B. Panigrahi, and T. Shripathi, J. Phys. Chem. Solids **61**, 1989 (2000).
[23] M. De Marco, D. Graf, J. Rijssenbeek, R. J. Cava, D. Z. Wang, Y. Tu, Z. F. Ren, J. H. Wang, M. Haka, S. Toorongian, M. J. Leone, and M. J. Naughton, Phys. Rev. B **60**, 7570 (1999).
[24] S. A. Carter, B. Batlogg, R. J. Cava, J. J. Krajewski, W. F. Peck, and L. W. Rupp, Phys. Rev. B **51**, 17184 (1995).

[25] S. Chikara, O. Korneta, W. P. Crummett, L. E. DeLong, P. Schlottmann, and G. Cao, Phys. Rev. B **80**, 140407 (2009).
[26] O. B. Korneta, T. Qi, S. Chikara, S. Parkin, L. E. De Long, P. Schlottmann, and G. Cao, Phys. Rev. B **82**, 115117 (2010).
[27] G. Sheldrick, Acta Crystallogr., Sect. A: Found. Crystallogr. **64**, 112 (2008).
[28] C. Dhital, T. Hogan, W. Zhou, X. Chen, Z. Ren, M. Pokharel, Y. Okada, M. Heine, W. Tian, Z. Yamani, C. Opeil, J. S. Helton, J. W. Lynn, Z. Wang, V. Madhavan, and S. D. Wilson, Nat. Commun. **5**, 3377 (2014).
[29] A. Glamazda, W. J. Lee, K. Y. Choi, P. Lemmens, H. Y. Choi, N. Lee, and Y. J. Choi, Phys. Rev. B **89**, 104406 (2014).
[30] G. Cao, J. E. Crow, R. P. Guertin, P. F. Henning, C. C. Homes, M. Strongin, D. N. Basov, and E. Lochner, Solid State Commun. **113**, 657 (2000).
[31] I. Franke, P. J. Baker, S. J. Blundell, T. Lancaster, W. Hayes, F. L. Pratt, and G. Cao, Phys. Rev. B **83**, 094416 (2011).
[32] V. K. S. Shante and S. Kirkpatrick, Adv. Phys. **20**, 325 (1971).
[33] S. J. Yuan, J. Terzic, J. C. Wang, L. Li, S. Aswartham, W. H. Song, F. Ye, and G. Cao, Phys. Rev. B **92**, 024425 (2015).